Nontrivial interplay of strong disorder and interactions in quantum spin-Hall insulators doped with dilute magnetic impurities

Jun-Hui Zheng[1,2,*] and Miguel A. Cazalilla[2,3,4,†]

[1]*Institut für Theoretische Physik, Goethe-Universität, 60438 Frankfurt/Main, Germany*

[2]*Department of Physics, National Tsing Hua University, Hsinchu 30013, Taiwan*

[3]*National Center for Theoretical Sciences (NCTS), Hsinchu 30013, Taiwan*

[4]*Donostia International Physics Center (DIPC), Manuel de Lardizabal, 4. 20018, San Sebastian, Spain*

(Received 29 September 2016; published 4 June 2018)

We investigate nonperturbatively the effect of a magnetic dopant impurity on the edge transport of a quantum spin Hall (QSH) insulator. We show that for a strongly coupled magnetic dopant located near the edge of a system, a pair of transmission antiresonances appear. When the chemical potential is on resonance, interaction effects broaden the antiresonance width with decreasing temperature, thus suppressing transport for both repulsive and moderately attractive interactions. Consequences for the recently observed QSH insulating phase of the 1-T′ of WTe_2 are briefly discussed.

DOI: 10.1103/PhysRevB.97.235402

I. INTRODUCTION

Two-dimensional (2D) topological materials like quantum spin Hall insulators (QSHIs) have become a fascinating research topic, with many potential applications [1–3]. Theoretically, QSHIs are predicted to possess gapless one-dimensional (1D) edge states [3,4]. Disorder potentials that are invariant under time-reversal symmetry (TRS) cannot cause Anderson localization, which is otherwise ubiquitous in 1D systems. Indeed, it has been shown [3–6] that for scalar and spin-orbit (SO) disorder potentials, even in the presence of weak electron-electron interactions, the 1D edge channels of QSHIs exhibit perfect transmission, whose hallmark is a quantized conductance at low temperatures [7]. On the other hand, strong interactions can break TRS [4,5] and lead to complex edge reconstructions [8,9], which jeopardize the perfect conductance quantization.

Experimentally, the QSH effect arising from gapless edge channels has been observed in HgTe/CdTe and InAs/GaSb/AlSb semiconductor quantum wells (QWs) [2], graphene submitted to a strong, tilted magnetic field [10], Bi (111) bilayers [11,12] and, more recently, in the 1-T′ phase of the transition metal dichalcogenide WTe_2 [13–16]. However, in HgTe/CdTe and InAs/GaSb/AlSb samples, long edge channels ($\sim 1\,\mu$m) in the topological phase exhibit relatively short mean-free paths, and the conductance deviates from quantization [2,17–19]. For the monolayer WTe_2, the conductance of the devices with longer edges does not exhibit the expected quantized value [14,16]. Moreover, the interpretation of the observations in InAs/GaSb QWs [18,19] has also been questioned after the discovery of rather similar edge-conduction features in the trivial phase [17].

Deviations from perfect conductance quantization at low temperatures arise from backscattering (BS) in the edge channels. Several BS mechanisms have been discussed using effective 1D models [3,20–24]. The latter often involve electron-electron scattering in combination with scalar, SO coupling and magnetic disorder [6,21–29]. Indeed, magnetic impurities break TRS above the Kondo temperature, and therefore they cause BS [5,28–31]. Nevertheless, the connection between the effective 1D models of disorder and the 2D aspects of the physics of QSHIs has not yet been fully investigated to the best of our knowledge. With the exception of a few numerical studies in the noninteracting limit [32,33], there appears to be no systematic investigation about the validity of these 1D models. Indeed, little is known about whether they actually apply in the strong coupling limit where coupling strength to the impurity becomes comparable or larger than the band gap of the QSHI. The latter is an experimentally relevant regime given the small band gaps exhibited by many of the experimentally realized QSHIs. Below, we shall show that the problem of a magnetic dopant impurity problem can be mapped, in the strong coupling limit, to a generalized 1D Fano model [34] describing two resonant levels coupled to an interacting 1D channel. Using an RG analysis, we show that the transmission coefficient is suppressed at low temperatures for repulsive interactions. Interestingly, when the chemical potential of the edge electrons resonates with one of the in-gap states, we find that the transmission is also suppressed for weak to moderately attractive interactions.

The rest of this paper is organized as follows: Sec. III describes the solution of the scattering problem for a toy model of a single magnetic impurity in the neighborhood of a noninteracting QSH edge channel. In Sec. IV, we construct an effective 1D model to describe this system, which allows us to treat the effect of weak to moderate interactions. In this section, we also discuss the effects not included in our toy model, such as the Rashba coupling in the band structure and the nonplanar alignment of the magnetic moment. Finally, in Sec. V, we offer

*jzheng@th.physik.uni-frankfurt.de

†miguel.cazalilla@gmail.com

the conclusions of this paper and provide an outlook for future research directions. The Appendix contains the most technical details of the calculations. Henceforth, we work in units where $\hbar = 1$.

II. MODEL

In this paper, we consider the effect of a magnetic dopant impurity in a QSHI, taking into account the electron-electron interactions along the edge. We shall assume a large spin-S magnetic impurity at temperatures T well above the Kondo temperature T_K (T_K is exponentially suppressed for large S [35]). This allows us to treat the magnetic moment of the dopant classically. For the sake of simplicity, we first solve a model in which the moment lies on the plane perpendicular to the spin-quantization axis of a QSHI, which is described by the Kane-Mele (KM) model [7]. The more general case when the magnetic moment is pointing in an arbitrary direction and the QSHI is described by more realistic extensions of the KM model will be discussed in Sec. IV C. Once the scattering problem with the dopant impurity is solved, we obtain an effective 1D model by fitting the scattering data. The effective model allows us to introduce the electron-electron interactions and treat them nonperturbatively.

With the above assumptions, the impurity potential is written as follows:

$$\mathcal{V}_{\rm imp} = \lambda_{\rm imp}(c^\dagger_{i_0\uparrow}c_{i_0\downarrow} + \text{H.c.}) = \lambda_{\rm imp}\, c^\dagger_{i_0} s^x c_{i_0}, \tag{1}$$

with $c^\dagger_i = (c^\dagger_{i\uparrow}, c^\dagger_{i\downarrow})$. As we will further elaborate below, for $\lambda_{\rm imp} \gg \Delta$, where 2Δ is the band gap, two bound states appear within the gap when the impurity is located deep inside the bulk of the QSHI. As the position of impurity is shifted from the bulk to the edge, the bound states hybridize with the edge states inducing a pair of antiresonances in the transmission coefficient. Thus, we show that the two-dimensionality arising from the QSHI physics leads to a much richer interplay between interactions and (magnetic) disorder than the one encountered in simple models of structureless impurities in 1D interacting electron systems [36–43]. These results provide the foundation for future studies based on more realistic models of the microscopic origins of the absence of quantization in the QSH effect at low temperatures.

Notice that the model considered here is also drastically different from models based on charge puddles resulting from doping fluctuations [23]. Indeed, the situation envisaged in this paper is more relevant to isolated strongly coupled magnetic moments that are well localized on the lattice scale, as is the case of vacancies in 2D materials [44] or isolated magnetic dopant impurities in general QSHIs. On the other hand, puddles are described [23] as extended quantum dots containing many levels and many electrons, which resonate with the QSH edge states. Furthermore, unlike the study reported below, the authors of Ref. [23] neglected Luttinger liquid effects in their treatment of the edge, which may be a good approximation for the HgTe QWs due to the large value of the dielectric constant. In the puddle model, BS is induced by the edge electrons dwelling in the quantum dots and undergoing inelastic scattering with other electrons in puddle [23]. Thus, in the absence of interactions, the puddle model will not lead to BS, whereas the model considered below BS is present even in the absence of interactions.

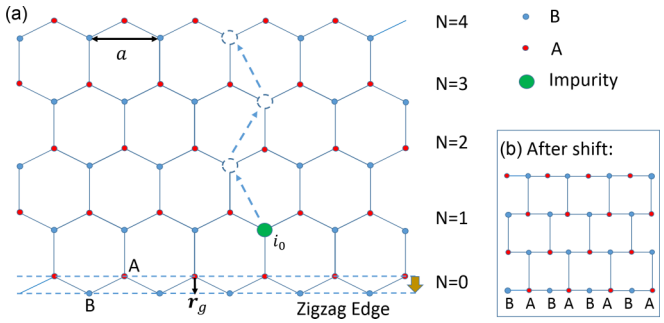

FIG. 1. Sketch of (a) the zigzag edge with a single impurity at the edge and (b) the "brick wall" lattice to which it maps.

III. SOLUTION OF SCATTERING PROBLEM

A. Solution of the clean Kane-Mele ribbon

To describe the QSHI, we consider the KM model [7] (cf. Fig. 1),

$$H_0 = -t\sum_{\langle i,j\rangle} c^\dagger_i c_j - i\lambda_{\rm SO}\sum_{\langle\langle i,j\rangle\rangle} \nu_{ij} c^\dagger_i s^z c_j, \tag{2}$$

where $\lambda_{\rm SO}$ describes the *intrinsic* SO coupling [7] as an imaginary next-nearest neighbor hopping and $\nu_{ij} = \pm 1$ depends on the electron hopping path; s^z is the electron spin projection on the axis perpendicular to the 2D plane. For the sake of simplicity, we first neglect Rashba SO coupling. This approximation does not qualitatively modify our results, as we discuss in Sec. V.

In the absence of interactions, the impurity problem is described by the Hamiltonian:

$$H = H_0 + \mathcal{V}_{\rm imp}. \tag{3}$$

To solve this problem, we first obtain an analytical solution of the *clean* KM model, Eq. (2), for a zigzag ribbon of width L (cf. Fig. 1). The transmission coefficient of the edge state for the system with an impurity Eq. (1) will be evaluated by solving the Lippmann-Schwinger equation (LSE) in Sec. III B.

In the ribbon geometry, the Bloch wave vector parallel to the edge, k_x, is a good quantum number. However, $k_y = -i\partial_y$ must be treated as an operator. The wave functions along the y axis obey open boundary conditions [45]. The Hamiltonian Eq. (2) in the Bloch basis can be obtained by using the Fourier transform,

$$c_{i\in A} = \sum_{\mathbf{k}} \frac{c_{\mathbf{k}A}}{\sqrt{N_t}} e^{i\mathbf{k}\cdot(\mathbf{R}_i+\mathbf{r}_g)}, \quad c_{i\in B} = \sum_{\mathbf{k}} \frac{c_{\mathbf{k}B}}{\sqrt{N_t}} e^{i\mathbf{k}\cdot\mathbf{R}_i}. \tag{4}$$

Here $\mathbf{R}_{i\in A(B)}$ is the position of $A(B)$ sublattice sites and N_t is the total number of unit cells. Because of the bipartite structure of the honeycomb lattice, the Fourier transform of H_0 is not unique and depends on the relative phase $\mathbf{k}\cdot\mathbf{r}_g$. This gauge freedom must be fixed by the boundary conditions (BCs). The appropriate choice for the zigzag edge is

$$\mathbf{r}_g = -(a/2\sqrt{3})\mathbf{e}_y, \tag{5}$$

so that the Nth row of the A sublattice are effectively shifted [see Eq. (4)] to overlap with the Nth row of the B sublattice (see Fig. 1). This maps the honeycomb lattice onto the so-called brick wall lattice and thus the BCs become

$$\Phi = (\Phi_B, \Phi_A)^T = 0 \text{ for } y = \pm L/2. \tag{6}$$

After identifying the BCs, we proceed to solve the 1D Schrödinger equation:

$$\mathcal{H}_0^s(\alpha, \hat{\beta})\Phi_s(k_x, y) = \epsilon \Phi_s(k_x, y), \tag{7}$$

where we have used the following notation: $\hat{\beta} = -i\frac{\sqrt{3}a}{2}\partial_y$ and $\mathcal{H}_0^s = \sum_i d_s^i \sigma^i$, with

$$\begin{aligned} d_s^x &= -t(2\cos\alpha + \cos\hat{\beta}), \\ d_s^y &= -t\sin\hat{\beta}, \\ d_s^z &= s\lambda_{\mathrm{SO}}(2\sin 2\alpha - 4\sin\alpha\cos\hat{\beta}), \end{aligned} \tag{8}$$

respectively, ($\alpha = k_x a/2$). The Pauli matrices σ^i ($i = x, y, z$) are in the pseudospin space corresponding to the sublattice (B, A) components. Furthermore, since s^z is a good quantum number, $s = \pm 1$. Below, we look for solutions that are combinations of plane waves $e^{ik_y y}$.

We are not interested in finite size effects and therefore take $L \to \infty$. In this limit, the coupling between the two edges vanishes and we obtain the dispersion for the edge states (see Appendix):

$$\epsilon_s(k_x) = \pm \frac{6s\lambda_{\mathrm{SO}} t \sin(k_x a)}{\sqrt{t^2 + [4\lambda_{\mathrm{SO}}\sin(k_x a/2)]^2}}, \tag{9}$$

where the $+$ $(-)$ sign corresponds to the bottom (top) edge at $y = -L/2$ ($y = +L/2$) and $s = \pm 1$. The bands of edge states cross at $k_x = \frac{\pi}{a}$ [7] (for a bearded edge, they cross at $k_x = 0$ [46], see Appendix). For $k_x \approx \frac{\pi}{a}$, Eq. (9) agrees with the semianalytic results of Ref. [47]. For the bottom edge states, below we use the notation $|k_x, s\rangle$. A plot of the bands [7] for a wide zigzag ribbon and the corresponding wave functions can be found in the Appendix.

B. Effect of the magnetic impurity

To investigate the effect of the impurity on the electronic transport, we next solve the LSE:

$$|\Psi\rangle = |\Phi\rangle + G_0(\epsilon)\mathcal{V}_{\mathrm{imp}}|\Psi\rangle, \tag{10}$$

where $G_0(\epsilon) = (\epsilon + i0^+ - H_0)^{-1}$ is the Green's function for Eq. (2). We assume the magnetic impurity to be located on the B sublattice at the bottom edge since the wave function of edge states on this edge is mostly localized on the B sublattice (see Appendix). To extract the transmission and reflection coefficients of the edge electrons, we assume the incident electron has a Bloch wave number k_x^0 on the right-moving edge channel, i.e., $|\Phi\rangle = |k_x^0, s = -1\rangle$. Therefore, its energy is $\epsilon_-(k_x^0)$ and its group velocity is $v = \partial_{k_x}\epsilon_-(k_x)|_{k_x = k_x^0}$. Let us introduce

$$\Phi(s\sigma, \mathbf{r}) = \langle s, \sigma, \mathbf{r}|\Phi\rangle, \tag{11}$$

$$\Psi(s\sigma, \mathbf{r}) = \langle s, \sigma, \mathbf{r}|\Psi\rangle, \tag{12}$$

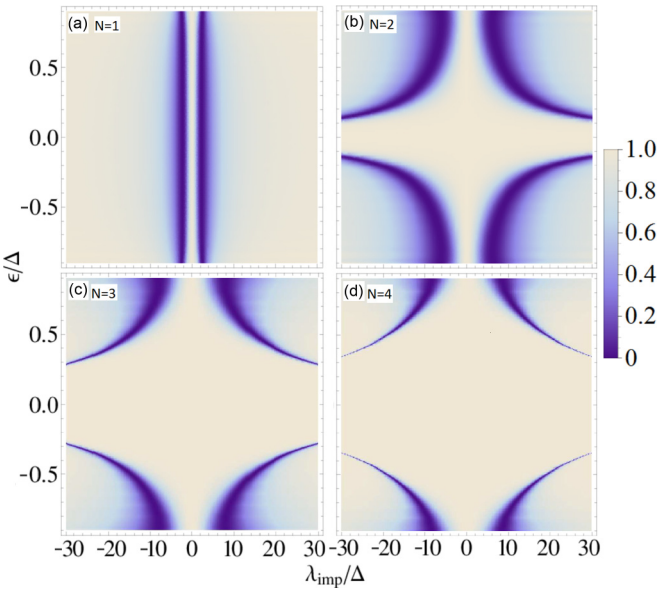

FIG. 2. Transmission coefficient $\mathcal{T}(\epsilon)$ for an impurity on a B sublattice site on (a) the first atomic row (i.e., $N = 1$), (b) $N = 2$, (c) $N = 3$, and (d) $N = 4$. The spin-orbit coupling is $\lambda_{\mathrm{SO}} = 0.06\,t$.

where $\sigma = (+, -)$ corresponds to the (B, A) sublattice. Thus, the asymptotic behavior of the wave function becomes

$$|\Psi\rangle \to (1 + \zeta_t)|\Phi\rangle \text{ for } x \to +\infty, \tag{13}$$

$$|\Psi\rangle \to |\Phi\rangle + \zeta_r|\tilde{\Phi}\rangle \text{ for } x \to -\infty, \tag{14}$$

where $|\tilde{\Phi}\rangle = |\frac{2\pi}{a} - k_x^0, s = +1\rangle$, and

$$\zeta_t = -i\lambda_{\mathrm{imp}} L_x \frac{\Psi(++, \mathbf{r}_0)\Phi^*(-+, \mathbf{r}_0)}{v}, \tag{15}$$

$$\zeta_r = -i\lambda_{\mathrm{imp}} L_x \frac{\Psi(-+, \mathbf{r}_0)\tilde{\Phi}^*(++, \mathbf{r}_0)}{v}. \tag{16}$$

Here L_x is the normalization length of system along the edge and $\mathbf{r}_0 \propto \mathbf{R}_{i_0}$ is the impurity position.

From the above results, the transmission and the reflection coefficients are obtained from ζ_r as follows:

$$\mathcal{T}(\epsilon) = |1 + \zeta_t|^2, \tag{17}$$

$$\mathcal{R}(\epsilon) = |\zeta_r|^2. \tag{18}$$

The energy dependence of the transmission coefficient is shown in Fig. 2. Note that, when the magnetic impurity is located on the first atomic row (i.e., $N = 1$), the transmission coefficient is essentially energy independent, which makes it similar to a BS impurity in a purely 1D channel. This behavior arises from weak coupling between the edge and bulk states via the impurity (owing to the small weight of the bulk states on the $N = 1$ row). This holds true even for relatively large values of λ_{imp}. Thus, scattering is dominated by the 1D edge states. However, we believe this behavior is not a robust feature but a peculiarity of the present KM model. On the other hand, for the second atomic row and beyond (i.e., $N \geqslant 2$), the weight of the bulk states is larger, and a strong impurity can thus lead to a sizable coupling between

bulk and edge states. As a consequence, for large values of $\lambda_{\rm imp}$, a pair of narrow scattering antiresonances appears within the energy gap. In the neighborhood of the antiresonances, the transmission coefficient changes very rapidly with energy and, on resonance, it vanishes for large $\lambda_{\rm imp}$.

To understand the emergence of the pair of scattering antiresonances, we need to consider the poles of the T-matrix,

$$T(\epsilon) = [\mathbf{1} - \mathcal{V}_{\rm imp} G_0(\epsilon)]^{-1} \mathcal{V}_{\rm imp}. \tag{19}$$

For a strong impurity potential located within the bulk of the QSHI, the poles of the T-matrix are obtained from the condition

$$\det\left[\mathbf{1} - \lambda_{\rm imp} G_0^B(\mathbf{r}_0,\mathbf{r}_0,\epsilon) s^x\right] = 0, \tag{20}$$

where G_0^B is the Green's function constructed from bulk states. The latter is real for ϵ within the energy gap since the density of states vanishes there and it is odd in ϵ (due to the particle-hole symmetry of H_0), therefore vanishing at $\epsilon = 0$, i.e., the middle of the gap. Thus, $G_0^B(\mathbf{r}_0,\mathbf{r}_0,\epsilon) \propto \epsilon$ for small ϵ. Hence, at large $\lambda_{\rm imp}$, two bound in-gap states appear at $\epsilon \propto \pm t^2/\lambda_{\rm imp}$, corresponding to the two eigenvalues of s^x. As the impurity location is shifted toward the edge, the bound states hybridize with the continuum of edge states, leading to the antiresonances in the transmission coefficient. We will generalize this argument below in Sec. IV C when discussing the effect of extensions to the present toy model.

IV. 1D EFFECTIVE MODEL

A. Noninteracting limit

After finding a nonperturbative solution to the scattering problem of the edge electrons with a magnetic dopant impurity, in this section we construct a 1D low-energy effective model that describes a noninteracting edge channel in the presence of magnetic impurity at large $\lambda_{\rm imp}/\Delta$, where $\Delta = 3\sqrt{3}\lambda_{\rm SO}$ (2Δ is the bulk band gap). The effective model is valid at energies and temperatures smaller than Δ and therefore only involves the degrees of freedom of the 1D edge and the in-gap states.

The Hamiltonian of the effective 1D model describing the coupling between the edge electrons and the in-gap states is constrained by the existence of a number of symmetries of $H = H_0 + \mathcal{V}_{\rm imp}$. The KM model in the ribbon geometry described by H_0 [cf. Eq. (2)], is invariant under TRS ($\mathcal{T}$), spin rotations about the z axis (i.e., $U_\theta = \exp(-i\theta s^z/2)$, $U_\theta^{-1} H_0 U_\theta = H_0$), particle-hole symmetry ($\mathcal{C}$), and lattice translations along the edge direction. The impurity potential, $\mathcal{V}_{\rm imp}$, breaks all those symmetries, but the composite system described by $H = H_0 + \mathcal{V}_{\rm imp}$ is invariant under the subgroup span by the combined $U_\pi\mathcal{T}$ and $\mathcal{CT}$ transformations. Therefore, according to the above discussion, the effective model takes the form of a generalized Fano model [34], describing two discrete levels coupled to the continuum of edge states. Furthermore, this model is invariant under $U_\pi\mathcal{T}$ and $\mathcal{CT}$. Since for $|\lambda_{\rm imp}| \to \infty$ the position of the resonances approaches the center of the band gap at $\epsilon = 0$, we shall focus in the neighborhood of $k_x = \frac{\pi}{a}$, where linearization of the edge state spectrum, i.e., $\epsilon_\pm(k_x) = \mp v_F k$, is a good approximation. Thus, the effective Hamiltonian can be written

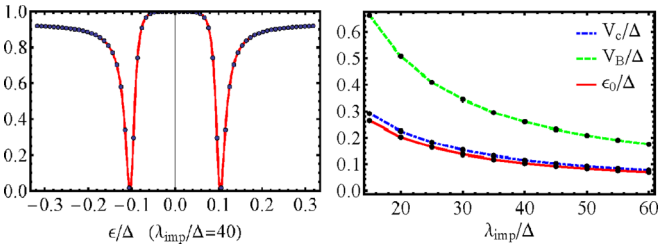

FIG. 3. Left: Transmission coefficient for an impurity strength $\lambda_{\rm imp} = 40\ \Delta$ (Δ is the band gap). Dots are the transmission coefficient obtained numerically for the Kane-Mele model with a backscatterer at the edge. The red line is the fit to the effective model [cf. Eq. (21)]. Right: Effective model parameters as a function of $\lambda_{\rm imp}$.

as follows:

$$H_{\rm eff} = H_B + H_+[u, t_+\psi(0)] + H_-[d, t_-\psi(0)], \tag{21}$$

$$H_B = i v_F \int dx\ \psi^\dagger s^z \partial_x \psi + V_B a_0 \psi^\dagger(0) s^x \psi(0), \tag{22}$$

$$H_\pm[f,\chi] = \pm\epsilon_0 \left(f^\dagger f - \tfrac{1}{2}\right) + V_c a_0^{1/2}[f^\dagger \chi + \text{H.c.}], \tag{23}$$

where $\psi^\dagger(x) = (\psi_L^\dagger(x), \psi_R^\dagger(x))$ is the spinor field operator describing the edge states, $u^\dagger$ and $d^\dagger$ are the creation operators of electrons in the bound states with s^x eigenvalue and energy $s^x = +1, \epsilon = +\epsilon_0$ and $s^x = -1, \epsilon = -\epsilon_0$, respectively, and $t_\pm = (\pm 1, 1)$; $a_0 = v_F/\Delta$ is a short distance cutoff. In the above model, V_B describes a renormalized BS amplitude for the edge electrons, and V_c the tunneling into and out of the bound states. The reflection coefficient for the effective 1D model reads:

$$\mathscr{R}(\epsilon) = \left| \sum_{p=\pm 1} \frac{p}{\frac{i V_c^2}{(\epsilon + p\epsilon_0)\Delta} + \left(1 - p\frac{i V_B}{2\Delta}\right)} \right|^2, \tag{24}$$

which accurately fits the results obtained (numerically) for $\mathcal{T}(\epsilon) = 1 - \mathscr{R}(\epsilon)$ from the nonperturbative solution of the scattering problem. The left panel of Fig. 3 shows the quality of fit of the transmission coefficient as a function of energy for a magnetic dopant impurity located in the second atomic row (i.e., $N = 2$). The behavior of the fitted parameters V_c, V_B, and ϵ_0 as functions of the impurity potential strength $\lambda_{\rm imp}$ is shown on the right panel. As expected from the above discussion, ϵ_0 decreases as $\lambda_{\rm imp} \to +\infty$. Note that $V_c, V_B \ll \Delta$, which is consistent with the assumption that the 1D model, Eq. (21) describes only the edge and in-gap states.

B. Interaction effects

Finally, we study the effect of electron interactions on the transport properties of the QSHI with a magnetic dopant. Interactions are treated nonperturbatively using the bosonization method [43]. Their characteristic energy scale is $\sim e^2/a_0$ (where e is the electron charge), which is assumed to be smaller than the band gap, 2Δ.

To apply bosonization to the interacting model, we further project the effective 1D model in Eq. (21) onto the subspace of excitations within the neighborhood of the Fermi energy, ϵ_F. In particular, when ϵ_F is away from $\pm\epsilon_0$, the bound states can be integrated out. To leading order, this yields a renormalized

BS amplitude,

$$V_B' \simeq V_B - \left[\frac{V_c^2}{\epsilon_0 - \epsilon_F} + \frac{V_c^2}{\epsilon_0 + \epsilon_F}\right], \tag{25}$$

and thus the 1D model reduces to the impurity model in a 1D interacting channel studied by Kane and Fisher [36,38] [cf. $H_{\rm KF}$ in Eq. (27) below] with an impurity potential whose BS amplitude $V_B = V_B'$.

On the other hand, on resonance, i.e., for $\epsilon_F \simeq +\epsilon_0$ ($\epsilon_F \simeq -\epsilon_0$), we can integrate out only the nonresonant level at $\epsilon_F \simeq -\epsilon_0$ ($\epsilon_F \simeq +\epsilon_0$). Assuming (without loss of generality) that $\epsilon_F \simeq -\epsilon_0$ yields the following low-energy effective model:

$$H_{\rm eff}' = H_{\rm KF} + H_-[d,t_-\psi(0)] + \left(d^\dagger d - \tfrac{1}{2}\right) \times [U_F\ \psi^\dagger(0)\psi(0) + U_B\ \psi^\dagger(0)s^x\psi(0)], \tag{26}$$

$$H_{\rm KF} = H_B + U\int dx\ \rho_R\rho_L. \tag{27}$$

The interactions between the edge electrons (with amplitude U) and between the edge electrons and the resonant level (with amplitudes U_F and U_B) have been included in the Hamiltonian. We note that integrating out the nonresonant level at $\epsilon = +\epsilon_0$ renormalizes the amplitude of $V_B - U_B/2$ in $H_{\rm eff}'$ by an amount $\simeq V_c^2/(\epsilon_F - \epsilon_0) \simeq -V_c^2/2\epsilon_0$. In addition, forward scattering is also generated but it is dropped since it can be eliminated by a unitary transformation [36,43].

The Hamiltonian $H_{\rm eff}'$ in Eqs. (26) and (27) is akin to a model of a (side-coupled) resonant level in an interacting 1D channel [48,49]. Thus, we apply an analysis similar to the one carried out by Goldstein and Berkovits in Ref. [48] to $H_{\rm eff}'$. After bosonizing [43] Eq. (26), we perform a unitary transformation to eliminate the forward interaction term $\propto U_F$ at the expense of renormalizing the scaling dimension (Δ_c) of the operator ($O_c \propto V_c$) describing the tunneling between the 1D edge channel and the resonant level. Thus,

$$\langle O_c^\dagger(\tau)O_c(0)\rangle \sim \frac{V_c^2}{\tau^{2\Delta_T}}, \tag{28}$$

where τ is the imaginary time and (see Ref. [48] and appendix) and

$$\Delta_T(K,U_F) = \tfrac{1}{4}\left[K + K^{-1}\left(1 - \tfrac{U_F K}{\pi v}\right)^2\right]. \tag{29}$$

In this expression,

$$K = \sqrt{\frac{2\pi v_F - U}{2\pi v_F + U}} \tag{30}$$

is the Luttinger parameter and

$$v = v_F\sqrt{1 - \left(\frac{U}{2\pi v_F}\right)^2} \tag{31}$$

the velocity of the edge plasmons [43]. Hence, tunneling into the resonant level becomes relevant in the renormalization-group (RG) sense for $\Delta_c(K,U_F) < 1$. There are two different interaction regimes for which this happens: For repulsive interactions (i.e., $K < 1$) and for weak to moderate attraction (i.e., $K \gtrsim 1$). In the former case, both tunneling V_c and the BS ($\propto V_B, U_F$) are renormalized to strong coupling by the charge-density wave fluctuations dominant in the 1D channel with $K < 1$ [43]. At $T = 0$, transmission through the edge channel is completely suppressed [48,49].

Interestingly, on resonance, the transmission through the edge channel of the QHSI is also suppressed for moderately attractive interactions i.e., $K \gtrsim 1$. In this regime, BS is *naïvely* irrelevant [36] and therefore U_B is initially suppressed by the dominant superconducting fluctuations in the edge channel (see below). However, the tunneling amplitude V_c is still a relevant perturbation since $\Delta_c(K,U_F) < 1$. Physically, this is because tunneling is a strongly relevant perturbation in 1D, also in the presence of interactions (see, e.g., Ref. [43], Chap. 8).

As the tunneling amplitude renormalizes to strong coupling with decreasing energy scale/temperature, the second-order RG flow equations (where $y_B \propto U_B$, $y_t \propto V_c$, $\delta_F \propto U_F$, etc. are dimensionless couplings, see Appendix D for derivation details):

$$\frac{dy_B}{d\ln\xi} = (1-K)y_B + y_t^2, \tag{32}$$

$$\frac{dy_t}{d\ln\xi} = [1 - K/4 - (1-\delta_F)^2K^{-1}/4]y_t + y_t(y_B + v_B), \tag{33}$$

$$\frac{d\delta_F}{d\ln\xi} = 4(1-\delta_F)y_t^2, \tag{34}$$

$$\frac{dv_B}{d\ln\xi} = (1-K)v_B, \tag{35}$$

show that this runaway flow of $y_t \propto V_c$ drags along both the BS amplitude $y_B \propto U_B$ and $\delta_F \propto U_F$. This ultimately leads to an effective suppression of the transmission through the edge channel as the temperature (or the energy scale) is reduced [48,49].

C. Rashba SOC and general magnetic moments

The main results obtained using the toy model introduced above can be easily generalized to account for the Rashba SO coupling in the band structure, i.e., adding to Eq. (2) a term of the form ($\mathbf{d}_{ij}$ is the vector joining the two nearest neighbor sites i and j on the honeycomb lattice):

$$H_R = i\lambda_r\sum_{\langle i,j\rangle} c_i^\dagger(\mathbf{s}\times\mathbf{d}_{ij})c_j, \tag{36}$$

and to the case of a more general coupling to the magnetic impurity ($\mathbf{n}$ is a unit vector):

$$\bar{\mathcal{V}}_{\rm imp} = \lambda_{\rm imp}c_{i_0}^\dagger(\mathbf{s}\cdot\mathbf{n})c_{i_0}. \tag{37}$$

In absence of Rashba and for $\mathbf{n}$ perpendicular to the spin-quantization z axis, we can implement rotation along s_z direction to change the magnetic moment in Eq. (37) to the form Eq. (1), which maps the problem to the toy model studied above.

The presence in the system of a uniform Rashba SOC, Eq. (37), violates the conservation of the total s_z as well as the particle-hole symmetry of the model. Yet, for weak to moderate Rashba SOC, the topological phase is stable and exhibits robust helical edge states [7]. In the following, we prove that in the limit $\lambda_{\rm imp} \to \infty$, a magnetic dopant impurity in the bulk still generates in-gap bound states, which can resonate with the

edge states when the impurity is located near the boundary of the insulator.

For an arbitrary orientation of the magnetic dopant in the bulk of a QSHI, the positions of bound states are determined by the equation [see Eq. (19)]

$$\det\left[\mathbf{1} - \lambda_{\rm imp}(\mathbf{n}\cdot\mathbf{s})G_0^B(\mathbf{r}_0,\mathbf{r}_0,\epsilon)\right] = 0, \tag{38}$$

where $G_0^B(\mathbf{r}_0,\mathbf{r}_0,\epsilon)$ is the local Green's function on the B sublattice, which is a 2×2 matrix in spin space. However, TRS implies that its off-diagonal elements vanish [50,51] $G^B_{0,\uparrow\downarrow}(\mathbf{r}_0,\mathbf{r}_0,\epsilon) = G^B_{0,\downarrow\uparrow}(\mathbf{r}_0,\mathbf{r}_0,\epsilon) = 0$ and $G^B_{0,\uparrow\uparrow}(\mathbf{r}_0,\mathbf{r}_0,\epsilon) = G^B_{0,\downarrow\downarrow}(\mathbf{r}_0,\mathbf{r}_0,\epsilon)$. Hence, $G_0^B(\mathbf{r}_0,\mathbf{r}_0,\epsilon)$ is indeed proportional to the unit matrix, i.e.,

$$G_0^B(\mathbf{r}_0,\mathbf{r}_0,\epsilon) = \frac{g_B(\epsilon)}{2}\,\mathbf{1}, \tag{39}$$

where the function $g_B(\epsilon)$ is related to the local density of states (LDOS) on the B sublattice. If we apply a rotation to align the spin quantization axis with the direction of $\mathbf{n}$, i.e., $U^\dagger(\mathbf{n})(\mathbf{n}\cdot\mathbf{s})U(\mathbf{n}) = s^z$, Eq. (38) yields the following conditions for the existence of in-gap bound states:

$$g_B(\epsilon) = \pm 2\lambda_{\rm imp}^{-1} \tag{40}$$

The function $g_B(\epsilon)$ becomes real for ϵ within the band gap because the LDOS vanishes there. In addition, since the LDOS is positive for ϵ outside the band gap, Kramers-Kronig relationships imply that $g_B(\epsilon)$ must have a zero within the gap, i.e., $g_B(\epsilon) = z^{-1}(\epsilon - \epsilon_c)$, where z^{-1} is the proportionally constant and ϵ_c is an energy within the band gap. For the KM model, particle-hole symmetry further requires that $\epsilon_c = 0$, which corresponds to the middle of the gap. Rashba SOC breaks particle-hole symmetry and, in general, we expect $\epsilon_c \neq 0$. Hence for sufficiently large $\lambda_{\rm imp}$, the in-gap states will be located at the energies:

$$\epsilon_0^{\pm} = \epsilon_c \pm \frac{2z}{\lambda_{\rm imp}}. \tag{41}$$

However, notice that for $\lambda_{\rm imp} \sim \Delta$ and/or large particle-hole asymmetry (i.e., $\epsilon_c \sim \Delta$), one or both solutions to Eq. (40) may not be real. Indeed, this the case when energy of the in-gap states overlaps with the continuum of states in the conduction or valence bands. However, the above analysis shows that for $\lambda_{\rm imp} \gg \Delta$, two in-gap states will always be present. The existence of the in-gap bound states can be further explicitly demonstrated by numerically computing the LDOS of QSHI in the presence of the magnetic dopant impurity. Figure 4 shows the results obtained for the KM with a Rashba SOC of $\lambda_r = 0.06t$ and $\mathbf{n}$ along the x axis. We have also checked the existence of the in-gap bound state(s) for other choices of λ_r and $\mathbf{n}$ (not shown here).

As the position of the magnetic impurity is shifted toward the edge, the in-gap states hybridize with the topological edge states, which results in antiresonances in edge channel transmission. This phenomenon is still described by the generalized Fano model introduced in Sec. III with different energy values for the energy of the in-gap state(s) and the tunneling V_c treated as an energy dependent function. Nevertheless, provided the Fermi level of the 1D edge (ϵ_F) is off resonance, both in-gap states can be integrated out, resulting in a local BS potential, which can be treated as a nonmagnetic impurity in an interacting 1D channel [7,39]. For ϵ_F on resonance with

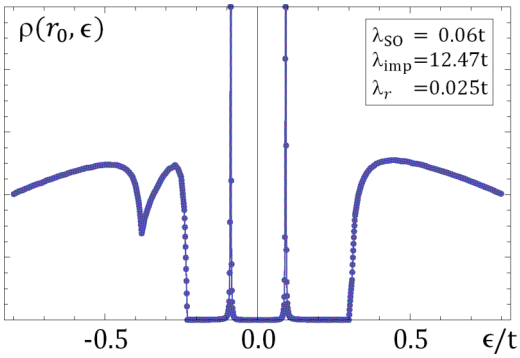

FIG. 4. Local density of states at the position of a magnetic dopant impurity located in the bulk of a QSHI insulator described by the Kane-Mele model [see Eqs. (2) and (36)] with a strength of the bulk Rashba spin-orbit coupling (SOC) $\lambda_r = 0.06t$. The impurity magnetic moment points along the x axis [see Eq. (1)]. Notice that the positions of the sharp peaks indicating the existence of impurity-induced in-gap states is not symmetrical with respect to the center of the band gap. This is a consequence of the particle-hole symmetry breaking caused by the Rashba (SOC).

one of the in-gap state(s), the other nonresonant state can be integrated out, giving rise to the similar model to the one studied at the end of Sec. IV B, $H'_{\rm eff}$ [cf. Eq. (27), the possible energy dependence of V_c being irrelevant in the RG sense]. A similar argument applies even when the impurity strength is not weak or the particle-hole symmetry strong, so that only one bound state exists. An exception to the phenomena described in the effective model of Eq. (27) is found when there is a symmetry that prevents the hybridization between the in-gap bound states and the electronic states at the edge. Although this is not generic, it is indeed the case for a dopant whose magnetic moment $\mathbf{n}$ points along the spin-quantization axis of the KM, Eq. (2). Thus, the total s^z is conserved and the Hilbert space of the problem splits into two subspaces labeled by different s^z without any matrix element connecting them. Thus, conservation of total s^z prevents the existence of BS [28].

Therefore, although we have based our calculations in a simplified model of the QSHI and the impurity, the phenomena described above does not depend on the specific microscopic details of the model in the large $\lambda_{\rm imp}$ limit. The emergence of transmission antiresonances and the interaction induced renormalization of the antiresonance linewidth [48,49] stems from the coupling between the edge states and the impurity-induced in-gap states. This will generically be present as long as the wave functions of the edge states and the states bound by the magnetic impurity overlap. Similar arguments can be applied to magnetic dopants described by more sophisticated models of of $\mathbb{Z}_2$ topological insulators. However, if $\lambda_{\rm imp}$ is decreased continuously, the bound states will merge into the continuum of bulk states (together or one by one, depending on the degree of particle-hole asymmetry) and finally the resonances will disappear.

V. SUMMARY AND OUTLOOK

In summary, we have investigated the transport properties of a QSHI in the presence of a strongly coupled magnetic

impurity. By obtaining a nonpertubative solution of the scattering problem, we have derived a 1D effective low-energy Hamiltonian describing the system. In the strong coupling limit, the impurity induces in-gap bound state, which, in proximity to the edge state, broadens into transmission antiresonances. When the chemical potential of the edge electrons is not resonant with any of the in-gap states induced by the magnetic impurity, the system can be effectively mapped to the problem of a nonmagnetic impurity in a Tomonaga-Luttinger liquid [36–38] with a renormalized BS strength at sufficiently low energy/temperatures (the latter energy scale being set by the separation between the Fermi level and the nearest resonant state). For strong attractive interactions in the channel, this suppression is absent and the 1D channel becomes increasingly transparent at low T. On the other hand, when the Fermi energy is on resonance, repulsive and weak to moderately attractive interactions lead to temperature-dependent broadening of the transmission antiresonance, which effectively suppresses the conductance of the edge channel as the temperature T is decreased.

For many of the current physical realizations of QSHIs [2,14,16], the regime in which $\lambda_{\rm imp} \gg \Delta$ is not at all unrealistic, as the size of the band gap is typically rather small [2,3,14–16], and its size can be tuned close to the topological transition. In addition, in 2D materials, localized moments can appear, e.g., from dangling bonds at vacancies [44], rather than from magnetic dopants alone. Based on the analysis provided here, we believe that the presence of such localized magnetic defects in proximity to the edge of the recently observed can induce significant BS in the newly observed QSHI in the 1-T′ phase of WTe_2. The mechanism described here provides additional BS sources to account for the experimentally observed [14,16] deviations from conductance quantization at low temperatures. Indeed, if the chemical potential of the edge electrons happens to be at (or near) resonance with in-gap states induced by a magnetic dopant, tunneling in/out of the in-gap states will suppress conductance through the edge channel more effectively than ordinary BS [for comparable strength of the bare BS y_B, v_B and tunneling y_t dimensionless couplings, cf. Eqs. (32) to (35)]. This is because tunneling in/out of the (nearly resonant) in-gap state is a more relevant perturbation than BS, as manifested by its smaller scaling dimension [i.e., typically $\Delta(K, U_F) < K$, cf. Eq. (29)], for both repulsive and moderately attractive interactions. A more detailed analysis relevant to this system will be reported in a future publication. Furthermore, in the future, we also plan to study extensions to the model studied here beyond the dilute impurity regime (i.e., the multi-impurity case). Another interesting direction is to treat the spin degrees of the magnetic impurity quantum mechanically. This is especially important to describe spin-$\frac{1}{2}$ impurities below the Kondo temperature. Finally, another interesting research direction, relevant to the study of Majorana bound states, is to the study of the competition of the type of magnetic disorder considered here and the proximity to a nearby s-wave superconductor [52].

ACKNOWLEDGMENTS

We thank L. Glazman, T. Giamarchi, F. Guinea, Y.-H. Ho, C.-L. Huang, S.-Q. Shen, and X.-P. Zhang for useful discussions. M.A.C. gratefully acknowledges support by the Ministry of Science and Technology (MOST) of Taiwan under Contract No. 102- 2112-M-007-024-MY5 and Taiwan's National Center of Theoretical Sciences (NCTS).

APPENDIX A: SPECTRUM AND WAVE FUNCTIONS

Here we provide the analytical approach to solve for the spectrum and the wave functions of both bulk and edge states for a generalized KM model [7],

$$\hat{H}_0 = -t \sum_{\langle i,j\rangle} c_i^\dagger c_j - i\lambda_{\rm SO} \sum_{\langle\langle i,j\rangle\rangle} \nu_{ij} c_i^\dagger s^z c_j + \lambda_v \sum_i \xi_i c_i^\dagger c_i, \tag{A1}$$

where a staggered potential with $\xi_i = +1$ for $\mathbf{R}_i \in B$ and $\xi_i = -1$ for $\mathbf{R}_i \in A$ sublattice has been included for generality. As mentioned in the main text, there is a gauge degree of freedom for the Fourier transformation of $\hat{c}_i^\dagger$ (or $\hat{c}_i$) due to the biparticle structure of the lattice. The gauge freedom allows us to effectively shift the lattice yielding different geometries for the edge.

Besides the zigzag edge of interest in the main text, it is also interesting to consider the beard edge in parallel. They correspond to two different gauge choices: (1) zigzag edge, $\mathbf{r}_g = -(a/2\sqrt{3})\mathbf{e}_y$, and (2) beard edge, $\mathbf{r}_g = (a/\sqrt{3})\mathbf{e}_y$. In our convention, $\sigma^z = (+,-)$ denotes the sublattice pseudospin components corresponding to the (B,A) sublattices.

1. Spectrum of edge states

For the case with zigzag edge, after the Fourier transformation, we obtain $\mathcal{H}_0^s(\alpha,\hat{\beta}) = \sum_i d_s^i \sigma^i$, we have used the notation where Pauli matrices σ^i $(i = x,y,z)$ is in the pseudospin space corresponding to the sublattice (B,A) components of the single-particle spin-wave function and

$$d_s^x = -t(2\cos\alpha + \cos\hat{\beta}), \tag{A2}$$

$$d_s^y = -t\sin\hat{\beta}, \tag{A3}$$

$$d_s^z = \lambda_v + s\lambda_{\rm SO}(2\sin 2\alpha - 4\sin\alpha\cos\hat{\beta}), \tag{A4}$$

with $\alpha = k_x a/2$, and $\hat{\beta} = -i\frac{\sqrt{3}a}{2}\partial_y$. We set $a = 1$ for simplicity. In addition, we treat $\hat{\beta}$ as an operator and β as its eigenvalues.

Substituting $\Phi_s(k_x, y) = \chi_s e^{\kappa y}$ to Eq. (7), we get the following secular equation:

$$Xf^2 + Yf + Z = 0, \tag{A5}$$

where the variables

$$f \equiv \cosh\frac{\sqrt{3}\kappa}{2}, \tag{A6}$$

$$X = -\left(4\lambda_{\rm SO}\sin\frac{k_x}{2}\right)^2, \tag{A7}$$

$$Y = 8s\lambda_{\rm SO}\sin\frac{k_x}{2}(\lambda_v + 2s\lambda_{\rm SO}\sin k_x) - 4t^2\cos\frac{k_x}{2}, \tag{A8}$$

$$Z = \epsilon^2 - t^2 - 4t^2\left(\cos\frac{k_x}{2}\right)^2 - (\lambda_v + 2s\lambda_{\rm SO}\sin k_x)^2. \tag{A9}$$

Hence, we obtain the following two roots:

$$f_{1,2} = (-Y \pm \sqrt{Y^2 - 4XZ})/2X, \tag{A10}$$

Thus, there are four roots for κ, corresponding to $\pm\kappa_{1,2}$ with $\kappa_{1,2} = \frac{2}{\sqrt{3}} \cosh^{-1} f_{1,2}$. For the edge states, we have that $\mathrm{Re}\,\kappa_{1,2} \neq 0$. Thus, we use the convention that $\mathrm{Re}\,\kappa_{1,2} > 0$ for the function $\kappa_{1,2} = \frac{2}{\sqrt{3}} \cosh^{-1} f_{1,2}$.

Note that only two linearly independent wave functions satisfy the open BCs corresponding the zigzag edge, namely $\Phi_s(k_x, \pm L/2) = 0$ for each value of ϵ. They are

$$g_c^1(k_x, y) - g_c^2(k_x, y), \tag{A11}$$

$$g_s^1(k_x, y) - g_s^2(k_x, y), \tag{A12}$$

where [45]

$$g_c^i(k_x, y) = \frac{\cosh(\kappa_i y)}{\cosh(\kappa_i L/2)}, \tag{A13}$$

$$g_s^i(k_x, y) = \frac{\sinh(\kappa_i y)}{\sinh(\kappa_i L/2)}. \tag{A14}$$

The eigenfunctions can be expressed as the linear combination of the above wave functions. By introducing a 2×2 matrix of coefficients $\mathcal{L} = [l_{ij}]$, the eigenfunctions can be written as follows:

$$\Phi_s(k_x, y) = \mathcal{L} \begin{bmatrix} g_c^1(k_x, y) - g_c^2(k_x, y) \\ g_s^1(k_x, y) - g_s^2(k_x, y) \end{bmatrix}. \tag{A15}$$

Substituting this function into Eq. (7), and using that $g_{c,s}^i$ are linearly independent, we obtain the following conditions relating the column vectors of the matrix $\mathcal{L}$:

$$\mathbf{L}_2 = \tanh(\kappa_1 L/2) M_1 \mathbf{L}_1, \tag{A16}$$

$$\mathbf{L}_2 = \tanh(\kappa_2 L/2) M_2 \mathbf{L}_1, \tag{A17}$$

$$\mathbf{L}_1 = \frac{1}{\tanh(\kappa_1 L/2)} M_1 \mathbf{L}_2, \tag{A18}$$

$$\mathbf{L}_1 = \frac{1}{\tanh(\kappa_2 L/2)} M_2 \mathbf{L}_2, \tag{A19}$$

where

$$\mathbf{L}_1 = (l_{11}, l_{21})^T, \tag{A20}$$

$$\mathbf{L}_2 = (l_{12}, l_{22})^T, \tag{A21}$$

$$M_i = \sigma^y \{(-2t \cos\alpha - t \cos\beta_i)\sigma^x + (\lambda_v + 2s\lambda_{\mathrm{SO}} \sin 2\alpha - 4s\lambda_{\mathrm{SO}} \sin\alpha \cos\beta_i)\sigma^z - \epsilon\}/(t \sin\beta_i), \tag{A22}$$

$$\beta_i = -i \frac{\sqrt{3}}{2} \kappa_i, \tag{A23}$$

respectively. Note that, in the above derivation, we have used the fact $\cos\hat{\beta} g_{c,s}^i(k_x, y) = \cos\beta_i g_{c,s}^i(k_x, y)$, $\sin\hat{\beta} g_c^i(k_x, y) = \sin\beta_i \tanh(\kappa_i L/2) g_s^i(k_x, y)$, and $\sin\hat{\beta}\, g_s^i(k_x, y) = \frac{\sin\beta_i}{\tanh(\kappa_i L/2)} g_c^i(k_x, y)$.

The combinations of equations in the same column in Eq. (A16) give the secular Eq. (A5), which relates κ_i and spectrum ϵ. The other two independent equations are obtained by combining diagonal terms in Eq. (A16), which yields

$$\mathbf{L}_2 = T M_1 M_2 \mathbf{L}_2 = \frac{1}{T} M_2 M_1 \mathbf{L}_2, \tag{A24}$$

where

$$T = \frac{\tanh(\kappa_1 L/2)}{\tanh(\kappa_2 L/2)}. \tag{A25}$$

Expressing κ_i as functions of ϵ, this equation is exactly the constraint for spectrum ϵ. In the following, we will solve this equation. Equation (A24) implies that

$$M_t \mathbf{L}_2 = 0, \tag{A26}$$

where $M_t \equiv T M_1 M_2 - \frac{1}{T} M_2 M_1$. To have a nontrivial solution for $\mathbf{L}_2$, the condition $\det M_t = 0$ is required, which gives

$$\left(T + \frac{1}{T}\right)^2 = 4D_0^2 \big/ \left(D_0^2 - D_x^2 - D_y^2 - D_z^2\right), \tag{A27}$$

where

$$D_x = t(\cos\beta_1 - \cos\beta_2)\epsilon, \tag{A28}$$

$$D_y = it(\lambda_v + 6s\lambda_{\mathrm{SO}} \sin 2\alpha)(\cos\beta_1 - \cos\beta_2), \tag{A29}$$

$$D_z = 4s\lambda_{\mathrm{SO}} \sin\alpha (\cos\beta_1 - \cos\beta_2)\epsilon, \tag{A30}$$

and $D_0 = t^2(2\cos\alpha + \cos\beta_1)(2\cos\alpha + \cos\beta_2) + (\lambda_v + 2s\lambda_{\mathrm{SO}} \sin 2\alpha - 4s\lambda_{\mathrm{SO}} \sin\alpha \cos\beta_1)(\lambda_v + 2s\lambda_{\mathrm{SO}} \sin 2\alpha - 4s\lambda_{\mathrm{SO}} \sin\alpha \cos\beta_2) - \epsilon^2$. For $L \to \infty$, $T = 1$ because $\mathrm{Re}\,\kappa_{1,2} > 0$. Thus, it becomes

$$D_x^2 + D_y^2 + D_z^2 = 0, \tag{A31}$$

which gives the dispersion

$$\epsilon_s^{\pm} = \pm \frac{t(\lambda_v + 6s\lambda_{\mathrm{SO}} \sin 2\alpha)}{\sqrt{t^2 + (4\lambda_{\mathrm{SO}} \sin\alpha)^2}}. \tag{A32}$$

Note that Eq. (A24) gives an additional constraint for the spectra. From $M_t \mathbf{L}_2 = 0$ and $T = 1$, we obtain

$$(D_x \sigma_x + D_y \sigma_y + D_z \sigma_z)\mathbf{L}_2 = 0. \tag{A33}$$

Combining it with $\mathbf{L}_2 = M_1 M_2 \mathbf{L}_2$ (Eq. (A24)), we obtain the following the constraint:

$$-D_0 = t^2 \sin\beta_1 \sin\beta_2. \tag{A34}$$

The second constraint is $\mathrm{Re}\,\kappa_{1,2} > 0$. These constraints restrict a region $k_x \in [\Lambda_s^-, \Lambda_s^+]$, where edge states exist. We show the resulted spectra in Fig. 5.

2. Wave functions for a semi-infinite system

To investigate the wave functions at one of the edges only, it is helpful to shift the coordinate origin so that the QSHI occupies the upper half plane ($0 \leqslant y \leqslant L$ with $L \to \infty$). For a semi-infinite system, the wave function satisfying the boundary condition $\Phi_{sk_x}(0) = \Phi_{sk_x}(L \to \infty) = 0$ has a much simpler form:

$$\Phi_{sk_x}(y) = C_s(k_x)\chi_s(k_x)(e^{-\kappa_{s,1} y} - e^{-\kappa_{s,2} y}). \tag{A35}$$

Thus, what is left is to determine the 2×1 matrix $\chi_s(k_x)$ and the normalization factor $C_s(k_x)$. For each k_x, we obtain the spectra

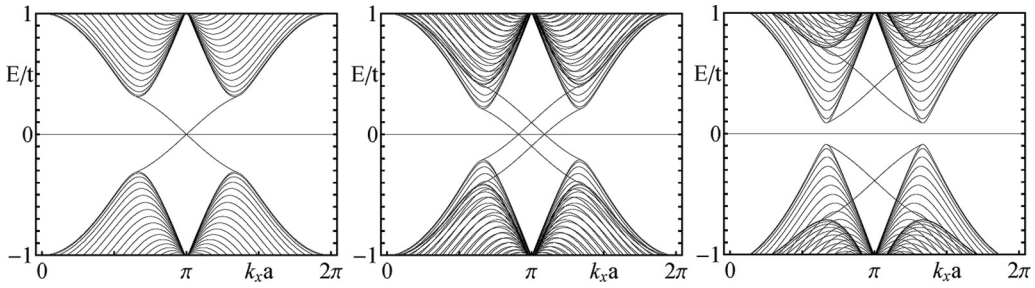

FIG. 5. Band structure of a zigzag ribbon described by Eq. (A1). Left panel: $\lambda_{SO} = 0.06t$ and $\lambda_v = 0$; central panel: $\lambda_{SO} = 0.06t$ and $\lambda_v = 0.1t < 3\sqrt{3}\lambda_{SO}$; right panel: $\lambda_{SO} = 0.06t$ and $\lambda_v = 0.4t > 3\sqrt{3}\lambda_{SO}$.

ϵ_s and the wave number $\kappa_{s,i} = \frac{2}{\sqrt{3}}\cosh^{-1} f_{s,i}$ with $i = 1,2$ in the last section. Substituting Eq. (A35) into the Schrödinger Eq. (7), we obtain

$$\chi_s(k_x) = \begin{bmatrix} -[\mathcal{H}_0^s]_{12}/\{[\mathcal{H}_0^s]_{11} - \epsilon_s\} \\ 1 \end{bmatrix} \equiv \begin{bmatrix} \chi_{s,1} \\ 1 \end{bmatrix}. \quad \text{(A36)}$$

Explicitly,

$$\chi_{s,1} = \frac{2t\cos\frac{k_x}{2} + t\exp(\sqrt{3}\kappa_{s,1}/2)}{\lambda_v + 2s\lambda_{SO}[\sin k_x - 2\sin(k_x/2)\cosh(\sqrt{3}\kappa_{s,1}/2)] - \epsilon_s}. \quad \text{(A37)}$$

Recall that the above wave functions only make sense when evaluated on the discrete set of points of the honeycomb lattice:

$$\psi_{sk_x}(n) = C_s(k_x)\chi_s(k_x)(e^{-\kappa_{s,1}ny_0} - e^{-\kappa_{s,2}ny_0}), \quad \text{(A38)}$$

where $y_0 = \sqrt{3}a/2$. The normalization factor is

$$C_s(k_x) = (1 + |\chi_{s,1}|^2)^{-1/2} C_s^0(k_x), \quad \text{(A39)}$$

where

$$C_s^0(k_x) = [\Upsilon(2\,\mathrm{Re}\,\kappa_{s,1}) + \Upsilon(2\,\mathrm{Re}\,\kappa_{s,2}) - \Upsilon(\kappa_{s,1}^* + \kappa_{s,2}) - \Upsilon(\kappa_{s,1} + \kappa_{s,2}^*)]^{-1/2}, \quad \text{(A40)}$$

and $\Upsilon(k) \equiv 1/[1 - \exp(-ky_0)]$. Upon denoting $\Phi_{sk_x,\sigma}(\mathbf{r})$ as the σ components of $\Phi_{sk_x}(\mathbf{r})$, we find $|\Phi_{sk_x,+}(\mathbf{r})|^2 \gg |\Phi_{sk_x,-}(\mathbf{r})|^2$ for the case $\lambda_v = 0$ and $\lambda_{SO} \ll t$, which suggests the bottom edge states "prefer" B-sublattice.

3. Wave functions for bulk states

For the bulk states with periodic boundary conditions, crystal momentum $\mathbf{k} = (k_x, k_y)$ is treated as a good quantum number in both the x direction and y direction. Thus, upon setting $\kappa = ik_y$ in Eq. (A5) (with $\beta = \frac{\sqrt{3}k_y}{2}$), we obtain the (bulk) dispersion:

$$E_{s\eta}(\mathbf{k}) = E_{s\eta}(k_x, k_y) = \eta\sqrt{t^2 + 4t^2\cos\alpha\cos\beta + 4t^2\cos^2\alpha + [\lambda_v + 2s\lambda_{SO}(\sin 2\alpha - 2\sin\alpha\cos\beta)]^2}, \quad \text{(A41)}$$

where $s, \eta = \pm 1$.

However, for open boundary conditions and in the limit $L \to \infty$, the spectrum of the bulk state is not modified from the above form because the boundary effects become negligible in the thermodynamic limit. On other hand, wave functions are modified and become different from Bloch waves because of the scattering with the boundary. Thus, from the secular Eq. (A5), for each $\kappa_1 = ik_y$ (k_y is real) and thus $f_1 \equiv \cos\frac{\sqrt{3}k_y}{2}$, we can find another root, $f_2 = -\frac{Y}{X} - f_1$. In total, four different roots for κ exist, i.e., $\pm\kappa_{1,2}$ with $\kappa_{1,2} = \frac{2}{\sqrt{3}}\cosh^{-1} f_{1,2}$, corresponding to a same energy ϵ. Note that f_1 and thus f_2 are real. Thus there are two different cases: (1) $|f_2| > 1$, the plane wave decays at the edge and (2) $|f_2| \leqslant 1$, different modes interference with each other:

Case 1: For $|f_2| > 1$, we have $\kappa_2 = \frac{2}{\sqrt{3}}\cosh^{-1} f_2$ with $\mathrm{Re}\,\kappa_2 > 0$. Thus the full solutions of the secular Eq. (A5) for κ are $\pm ik_y$ and $\pm\kappa_2$. The mode $\sim e^{\kappa_2 y}$ diverges for $y \to \infty$, so it will not emerge and there are only there modes left: $e^{\pm\kappa_1 y}$ and $e^{-\kappa_2 y}$. After using the boundary condition $\Phi_{s\eta,\mathbf{k}}(y = 0) = 0$, only two linear independent wave functions are left. The general wave function has the following form:

$$\Phi_{s\eta,\mathbf{k}}(y) = \frac{C_{s\eta}(\mathbf{k})}{\sqrt{N_y}}\mathcal{L}\begin{bmatrix} \exp(ik_y y) - \exp(-\kappa_2 y) \\ \exp(-ik_y y) - \exp(-\kappa_2 y) \end{bmatrix}, \quad \text{(A42)}$$

where $\mathcal{L} = [l_{ij}]_{2\times 2}$ is a 2×2 matrix, and $C_{s\eta}(\mathbf{k})$ is the normalization constant. Obviously, such a kind of wave function is a combination of the extended state and local state, which decays at the edge.

Now we need to calculate out the matrix $\mathcal{L}$. Substituting Eq. (A42) into Schrödinger Eq. (7), and using the fact that $\exp(\pm ik_y y)$ and $\exp(-\kappa_2 y)$ are linear independent, we obtain the following results:

$$\mathbf{L}_1 = c_1\begin{bmatrix} l_1 \\ 1 \end{bmatrix}, \quad \mathbf{L}_2 = c_2\begin{bmatrix} l_1^* \\ 1 \end{bmatrix}, \quad \text{(A43)}$$

$$\mathbf{L}_1 + \mathbf{L}_2 = \begin{bmatrix} l_2 \\ 1 \end{bmatrix}, \quad \text{(A44)}$$

where

$$\mathbf{L}_1 = (l_{11}, l_{21})^T, \tag{A45}$$

$$\mathbf{L}_2 = (l_{12}, l_{22})^T, \tag{A46}$$

$$l_i = -\frac{\left[\mathcal{H}_0^s(\alpha,\beta_i)\right]_{12}}{\left[\mathcal{H}_0^s(\alpha,\beta_i)\right]_{11} - E_{s\eta}(\mathbf{k})}, \tag{A47}$$

and c_1, c_2 are constants, $\beta_1 = \frac{\sqrt{3}}{2}k_y$, $\beta_2 = i\frac{\sqrt{3}}{2}\kappa_2$. Solving these equations, we find $c_1 = \frac{l_2 - l_1^*}{l_1 - l_1^*}$ and $c_2 = \frac{-l_2 + l_1}{l_1 - l_1^*}$.

The next step is to calculate the normalization coefficient $C_{s\eta}(\mathbf{k})$. For large L limit, $\exp(-\kappa_2 y)$ does not influence normalization. Using the orthogonality of $\exp(\pm i k_y y)$, we obtain

$$C_{s\eta}(\mathbf{k}) = \frac{1}{\sqrt{|c_1|^2 + |c_2|^2}\sqrt{|l_1|^2 + 1}}. \tag{A48}$$

As a result, in real space, we have

$$\Phi_{s\eta,\mathbf{k}}(n) = \frac{C_{s\eta}(\mathbf{k})}{\sqrt{N_y}}\mathcal{L}\begin{bmatrix} \exp(ik_y n y_0) - \exp(-\kappa_2 n y_0) \\ \exp(-ik_y n y_0) - \exp(-\kappa_2 n y_0) \end{bmatrix}. \tag{A49}$$

Case 2: For $|f_2| \leqslant 1$, we have $\kappa_2 = \frac{2}{\sqrt{3}}\cosh^{-1} f_2 = ik_y'$ with $k_y' \geqslant 0$. The full solutions of the secular Eq. (A5) for κ are $\pm ik_y$ and $\pm ik_y'$. The boundary conditions $\Phi_{s\eta,\mathbf{k}}(y = 0) = 0$ require these four running waves inference with each other, and thus there are only three linear independent wave functions. Following the method used in the previous case, we can construct the eigenfunctions by combining the three wave functions. However, we shall proceed in a different way here. Similar to the previous case, there is one eigenfunction,

$$|1\rangle = \frac{1}{\sqrt{N_y}}C_{s\eta}(\mathbf{k})\mathcal{L}\begin{bmatrix} \exp(ik_y y) - \exp(-ik_y' y) \\ \exp(-ik_y y) - \exp(-ik_y' y) \end{bmatrix}, \tag{A50}$$

where $\mathcal{L}$ is same as the one in Eq. (A42) except for the replacement of κ_2 with ik_y' and thus the normalization becomes

$$C_{s\eta}(\mathbf{k}) = \frac{1}{\sqrt{(|c_1|^2 + |c_2|^2)(|l_1|^2 + 1) + (|l_2|^2 + 1)}}. \tag{A51}$$

The second eigenstate $|2\rangle$ can be obtained by the replacements: $k_y \to k_y'$ (which implies that $l_2 \to l_1^*$). We denote the corresponding parameters as $\mathbf{L}_1'$, $\mathbf{L}_2'$, c_1', c_2', and $C_{s\eta}(\mathbf{k}')$. Note that these two eigenstates are not orthogonal.

In the following, we construct an orthogonal and symmetric basis by means of

$$|+\rangle = |1\rangle + \vartheta|2\rangle, \quad |-\rangle = |2\rangle + \vartheta|1\rangle. \tag{A52}$$

Using the orthogonality condition together with $\langle 1|1\rangle = \langle 2|2\rangle = 1$, we obtain

$$|\vartheta|^2 = 1, \ \ \mathrm{Re}\,\vartheta = -\mathrm{Re}\,\langle 1|2\rangle, \tag{A53}$$

where $\langle 1|2\rangle = C_{s\eta}(\mathbf{k})C_{s\eta}(\mathbf{k}')[-c_2^*(|l_1|^2 + 1) - c_2'(|l_2|^2 + 1)]$. We use the convention that $\mathrm{Im}\,\vartheta = \sqrt{1 - (\mathrm{Re}\,\vartheta)^2} \geqslant 0$, and finally, we obtain the orthonormalized wave functions:

$$\Phi_{s\eta\mathbf{k}}(n) = \frac{1}{\sqrt{2 + 2\mathrm{Re}d[\vartheta\langle 1|2\rangle]}}|+\rangle, \tag{A54}$$

$$\Phi_{s\eta\mathbf{k}'}(n) = \frac{1}{\sqrt{2 + 2\mathrm{Re}[\vartheta\langle 2|1\rangle]}}|-\rangle. \tag{A55}$$

APPENDIX B: GREEN'S FUNCTION FOR THE KANE-MELE MODEL IN A SEMI-INFINITE SYSTEM

So far, we have obtained the eigenvalues and the complete set of eigenfunctions for the model of Eq. (A1). Hence, the Green's function can be expressed in terms of them:

$$\hat{G}_0(\epsilon) = \sum_{\mathbf{k},s\eta}\frac{|\mathbf{k},s,\eta\rangle\langle\mathbf{k},s,\eta|}{\epsilon + i0^+ - E_{s\eta}(\mathbf{k})} + \sum_{k_x,s}\frac{|k_x,s\rangle\langle k_x,s|}{\epsilon + i0^+ - \epsilon_s(k_x)}, \tag{B1}$$

where $|\mathbf{k},s,\eta\rangle = \Phi_{s\eta\mathbf{k}}$. In the real space,

$$G^s_{0,\sigma\sigma'}(\mathbf{r},\mathbf{r}',\epsilon) = \langle\mathbf{r},s,\sigma|\hat{G}_0(\epsilon)|\mathbf{r}',s,\sigma'\rangle, \tag{B2}$$

where $\sigma = \pm 1$ represents the different components of σ^z. Thus, using $\langle\mathbf{r},s,\sigma|\mathbf{k},s,\eta\rangle = \Phi_{s\eta\mathbf{k},\sigma}(\mathbf{r})$ and $\langle\mathbf{r},s,\sigma|k_x,s\rangle = \Phi_{sk_x,\sigma}(\mathbf{r})$, where $\Phi_{s\eta\mathbf{k},\sigma}(\mathbf{r})$ and $\Phi_{sk_x,\sigma}(\mathbf{r})$ are the σ components of $\Phi_{s\eta\mathbf{k}}(\mathbf{r})$ and $\Phi_{sk_x}(\mathbf{r})$ respectively, we have

$$G^s_{0,\sigma\sigma'}(\mathbf{r},\mathbf{r}',\epsilon) = \sum_{\mathbf{k},\eta}\frac{\Phi_{s\eta\mathbf{k},\sigma}(\mathbf{r})\Phi^*_{s\eta\mathbf{k},\sigma'}(\mathbf{r}')}{\epsilon + i0^+ - E_{s\eta}(\mathbf{k})} + \sum_{k_x}\frac{\Phi_{sk_x,\sigma}(\mathbf{r})\Phi^*_{sk_x,\sigma'}(\mathbf{r}')}{\epsilon + i0^+ - \epsilon_s(k_x)}. \tag{B3}$$

APPENDIX C: SPECTRUM OF THE BEARD EDGE

For comparison purposes, we also study the edge spectrum for the beard edge. Using a gauge choice where $\mathbf{r}_g = (a/\sqrt{3})\mathbf{e}_y$, and following the same steps as for the zigzag case, we obtain the spectrum for the edge state:

$$\epsilon_s^{\pm} = \pm\frac{t[2s\lambda_{\mathrm{SO}}\sin\alpha + \cos\alpha(\lambda_v + 2s\lambda_{\mathrm{SO}}\sin 2\alpha)]}{\sqrt{(t\cos\alpha)^2 + (2\lambda_{\mathrm{SO}}\sin\alpha)^2}}. \tag{C1}$$

In this case, the constraint becomes

$$-D_0 = 4t^2\cos^2\alpha\sin\beta_1\sin\beta_2, \tag{C2}$$

where

$$\begin{aligned} D_0 &= t^2 w_1 w_2 + u_1 u_2 - \epsilon^2, \\ w_i &= 1 + 2\cos\alpha\cos\beta_i, \\ u_i &= \lambda_v + 2s\lambda_{\mathrm{SO}}\sin 2\alpha - 4s\lambda_{\mathrm{SO}}\sin\alpha\cos\beta_i. \end{aligned} \tag{C3}$$

The resulting band structure is shown in Fig. 6. Note that the edge states intersect at $k_x = 0$ [46].

APPENDIX D: RENORMALIZATION GROUP ANALYSIS

Next, to deal with the effects of interactions in a nonperturbative way, we shall rely upon the bosonization technique. The resulting model is analyzed along the lines of the analysis reported in Ref. [48].

In bosonization, the electron field operator for the right- (R) and left-moving (L) edge electron can be expressed in terms

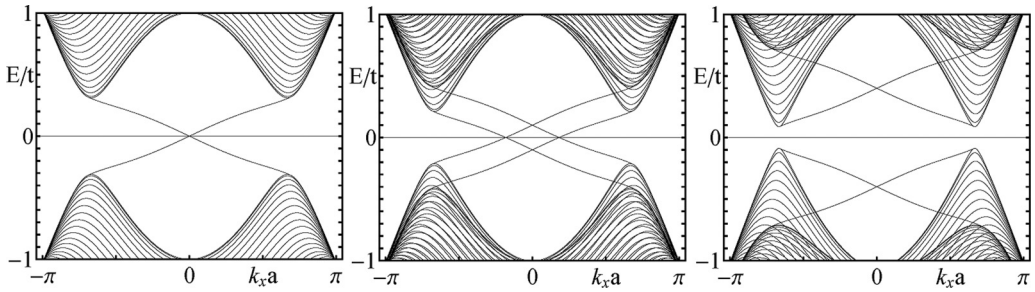

FIG. 6. Band structure of a bearded-edge ribbon described by Eq. (A1). Left panel: $\lambda_{SO} = 0.06t$ and $\lambda_v = 0$; central panel: $\lambda_{SO} = 0.06t$ and $\lambda_v = 0.1t < 3\sqrt{3}\lambda_{SO}$; right panel: $\lambda_{SO} = 0.06t$ and $\lambda_v = 0.4t > 3\sqrt{3}\lambda_{SO}$.

of a set of bosonic fields $\theta(x)$ and $\phi(x)$ as follows:

$$\psi_{R(L)}(x) = \frac{U_{R(L)}}{\sqrt{2\pi\upsilon\xi}} e^{-i[\pm\phi(x)-\theta(x)]}, \tag{D1}$$

where ξ is a short-distance cutoff, υ is the plasmon velocity [cf. Eq. (31)], U_R and U_L are the so-called Klein factors satisfying $\{U_r, U_{r'}\} = 2\delta_{r,r'}$, which allows us to satisfy the anticommutation relations between the two fermion chiralities R and L. The bosonic fields obey

$$[\phi(x),\theta(x')] = i\frac{\pi}{2}\mathrm{sgn}(x'-x). \tag{D2}$$

The chiral densities are given by

$$\rho_{R(L)}(x) = -\frac{1}{2\pi}(\partial_x\phi \mp \partial_x\theta). \tag{D3}$$

After bosonizing the low-energy effective model and upon applying a unitary transformation generated by

$$S = \exp[i\zeta\theta_0,] \tag{D4}$$

with $\zeta = \delta_F(d^\dagger d - \frac{1}{2})$, $\delta_F = \frac{KU_F}{\pi\upsilon}$, and using the factor $e^{-i\zeta\theta(0)}\partial_x\phi(x)e^{i\zeta\theta(0)} = \partial_x\phi(x) - i\zeta[\theta(0),\partial_x\phi(x)] = \partial_x\phi(x) + \zeta\pi\delta(x)$, the forward scattering term $\propto U_F$ can be eliminated from H'_{eff} [cf. Eq. (27)], and the resulting Hamitonian, $H''_{\mathrm{eff}} = S^\dagger H'_{\mathrm{eff}} S$ reads

$$\begin{aligned} H''_{\mathrm{eff}} = H_* &+ \frac{\upsilon_B}{\xi}[U_R U_L e^{2i\phi_0} + U_L U_R e^{-2i\phi_0}] \\ &+ \frac{2y_B}{\xi}\left(d^\dagger d - \frac{1}{2}\right)[U_R U_L e^{2i\phi_0} + U_L U_R e^{-2i\phi_0}] \\ &+ \frac{y_t}{\xi}[d^\dagger(U_R e^{-i(\phi_0-\lambda\theta_0)} - U_L e^{i(\phi_0+\lambda\theta_0)}) \\ &+ (U_R e^{i(\phi_0-\lambda\theta_0)} - U_L e^{-i(\phi_0+\lambda\theta_0)})d], \end{aligned} \tag{D5}$$

where

$$H_* = \frac{\upsilon}{2\pi}\int dx[K(\partial_x\theta)^2 + K^{-1}(\partial_x\phi)^2] - \varepsilon_0\left(d^\dagger d - \frac{1}{2}\right). \tag{D6}$$

Here ε_0 denotes the distance of the bound state from the Fermi energy of the edge channel, ϵ_F. In what follows, we focus on the resonant case for which $\epsilon_0 = 0$. In addition, $\lambda = 1 - \delta_F$, $\phi_0 = \phi(x = 0)$, $\theta_0 = \theta(x = 0)$, υ_B, y_B, y_t are dimensionless couplings, and K is the Luttinger parameter, and υ is the edge plasmon velocity.

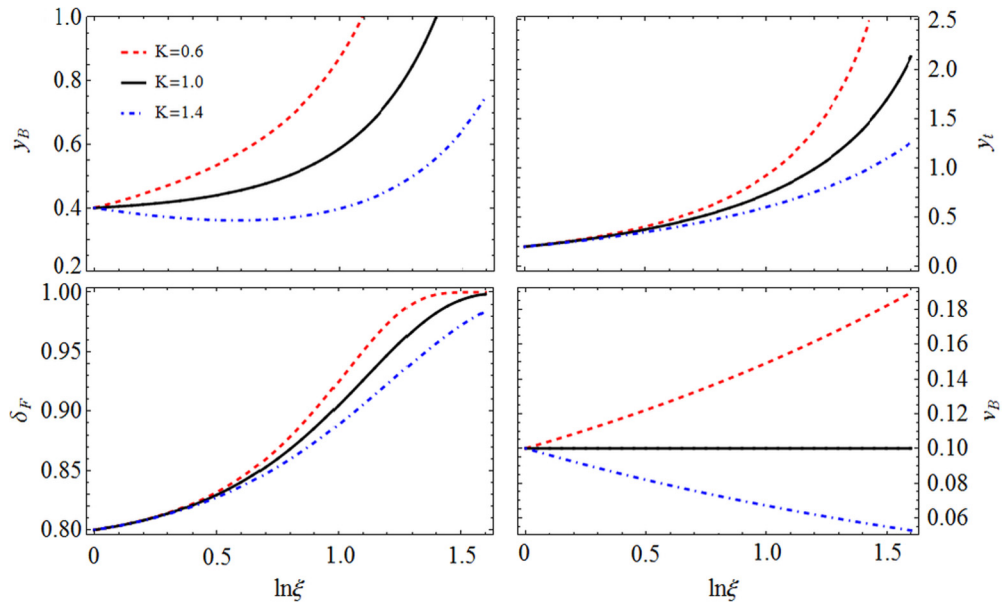

FIG. 7. The sketch of the RG flows for the couplings that parametrize the effective low-energy model.

Using Cardy's approach [53] and taking into account that

$$\langle e^{2i\phi_0(\tau)} e^{-2i\phi_0(0)} \rangle \sim |\tau|^{-2K}, \tag{D7}$$

$$\langle e^{i[\phi_0(\tau)-\lambda\theta_0(\tau)]} e^{-i[\phi_0(0)-\lambda\theta_0(0)]} \rangle \sim |\tau|^{-\alpha(K,\lambda)}, \tag{D8}$$

$$\alpha(K,\lambda) = \frac{K}{2} + \frac{\lambda^2 K^{-1}}{2}, \tag{D9}$$

we arrive at the set of RG equations valid to second order in the couplings describing BS and tunneling in and out of the resonant level given in Eqs. (32)–(35). The RG equations are similar to those derived in Ref. [48] for a model of a resonant level that is side-coupled to an interacting 1D electron system. As described in the main text, the equations show that for weak to moderate attractive interactions (i.e., $K \gtrsim 1$), the tunneling operator $\propto y_t$ is flows to strong coupling. On the other hand, both the BS interaction ($\propto y_B$) and potential ($\propto v_B$) will be initially suppressed. Eventually, the runaway flow of y_t drags along δ_F and y_B, quickly driving the forward interaction with the level to its fixed point $\delta_F^* = 1$. As a result, the transmission through the impurity will be suppressed, as discussed in the main text.

Figure 7 shows a sketch of the typical RG flows for moderately repulsive (i.e., $K \lesssim 1$) and moderately attractive (i.e., $K \gtrsim 1$) interactions. In both regimes, all couplings [except for the BS potential v_B for $K > 1$, cf Eq. (35)] rapidly reach values of order unity, which, in the perturbative approach, corresponds to a runaway flow to strong coupling.

[1] M. Z. Hasan and C. L. Kane, Rev. Mod. Phys. **82**, 3045 (2010); X.-L. Qi and S.-C. Zhang, *ibid.* **83**, 1057 (2011).

[2] M. König, S. Wiedmann, C. Brüne, A. Roth, H. Buhmann, L. W. Molenkamp, X.-L. Qi, and S.-C. Zhang, Science **318**, 766 (2007); A. Roth, C. Brüne, H. Buhmann, L. W. Molenkamp, J. Maciejko, X.-L. Qi, and S.-C. Zhang, *ibid.* **325**, 294 (2009); K. C. Nowack, E. M. Spanton, M. Baenninger, M. König, J. R. Kirtley, B. Kalisky, C. Ames, P. Leubner, C. Brüne, H. Buhmann, L. W. Molenkamp, D. Goldhaber-Gordon, and K. A. Moler, Nat. Mater. **12**, 787 (2013); G. Grabecki, J. Wróbel, M. Czapkiewicz, Ł. Cywiński, S. Gierałtowska, E. Guziewicz, M. Zholudev, V. Gavrilenko, N. N. Mikhailov, S. A. Dvoretski, F. Teppe, W. Knap, and T. Dietl, Phys. Rev. B **88**, 165309 (2013); G. M. Gusev, Z. D. Kvon, E. B. Olshanetsky, A. D. Levin, Y. Krupko, J. C. Portal, N. N. Mikhailov, and S. A. Dvoretsky, *ibid.* **89**, 125305 (2014); I. Knez, R.-R. Du, and G. Sullivan, Phys. Rev. Lett. **107**, 136603 (2011); K. Suzuki, Y. Harada, K. Onomitsu, and K. Muraki, Phys. Rev. B **87**, 235311 (2013); I. Knez, C. T. Rettner, S.-H. Yang, S. S. P. Parkin, L. Du, R.-R. Du, and G. Sullivan, Phys. Rev. Lett. **112**, 026602 (2014); E. M. Spanton, K. C. Nowack, L. Du, G. Sullivan, R.-R. Du, and K. A. Moler, *ibid.* **113**, 026804 (2014).

[3] G. Dolcetto, M. Sassetti, and T. L. Schmidt, Rivista del Nuovo Cimento **39**, 113 (2016).

[4] C. Xu and J. E. Moore, Phys. Rev. B **73**, 045322 (2006).

[5] C. Wu, B. A. Bernevig, and S. C. Zhang, Phys. Rev. Lett. **96**, 106401 (2006).

[6] A. Ström, H. Johannesson, and G. I. Japaridze, Phys. Rev. Lett. **104**, 256804 (2010).

[7] C. L. Kane and E. J. Mele, Phys. Rev. Lett. **95**, 226801 (2005); **95**, 146802 (2005).

[8] J. Wang, Y. Meir, and Y. Gefen, Phys. Rev. Lett. **118**, 046801 (2017).

[9] A. Amaricci, L. Privitera, F. Petocchi, M. Capone, G. Sangiovanni, and B. Trauzettel, Phys. Rev. B **95**, 205120 (2017).

[10] A. F. Young, J. D. Sanchez-Yamagishi, B. Hunt, S. H. Choi, K. Watanabe, T. Taniguchi, R. C. Ashoori, and P. Jarillo-Herrero, Nature **505**, 528 (2014).

[11] F. Yang, L. Miao, Z. F. Wang, M.-Y. Yao, F. Zhu, Y. R. Song, M.-X. Wang, J.-P. Xu, A. V. Fedorov, Z. Sun, G. B. Zhang, C. Liu, F. Liu, D. Qian, C. L. Gao, and J.-F. Jia, Phys. Rev. Lett. **109**, 016801 (2012).

[12] I. K. Drozdov, A. Alexandradinata, S. Jeon, S. Nadj-Perge, H. Ji, R. J. Cava, A. Bernevig, and A. Yazdani, Nat. Phys. **10**, 664 (2014).

[13] X. Qian, J. Liu, L. Fu, and J. Li, Science **346**, 1344 (2014).

[14] Z. Fei, T. Palomaki, S. Wu, W. Zhao, X. Cai, B. Sun, P. Nguyen, J. Finney, X. Xu, and D. H. Cobden, Nat. Phys. **13**, 677 (2017).

[15] S. Tang, C. Zhang, D. Wong, Z. Pedramrazi, H.-Z. Tsai, C. Jia, B. Moritz, M. Claassen, H. Ryu, S. Kahn, J. Jiang, H. Yan, M. Hashimoto, D. Lu, R. G. Moore, C.-C. Hwang, C. Hwang, Z. Hussain, Y. Chen, M. M. Ugeda, Z. Liu, X. Xie, T. P. Devereaux, M. F. Crommie, S.-K. Mo, and Z.-X. Shen, Nat. Phys. **13**, 683 (2017).

[16] S. Wu, V. Fatemi, Q. D. Gibson, K. Watanabe, T. Taniguchi, R. J. Cava, and P. Jarillo-Herrero, Science **359**, 76 (2018).

[17] F. Nichele, H. J. Suominen, M. Kjaergaard, C. M. Marcus, E. Sajadi, J. A. Folk, F. Qu, A. J. A. Beukman, F. K. de Vries, J. van Veen, S. Nadj-Perge, L. P. Kouwenhoven, B.-M. Nguyen, A. A Kiselev, W. Yi, M. Sokolich, M. J. Manfra, E. M. Spanton, and K. A. Moler, New J. Phys. **18**, 083005 (2016).

[18] T. Li, P. Wang, H. Fu, L. Du, K. A. Schreiber, X. Mu, X. Liu, G. Sullivan, G. A. Csáthy, X. Lin, and R.-R. Du, Phys. Rev. Lett. **115**, 136804 (2015).

[19] L. Du, T. Li, W. Lou, X. Wu, X. Liu, Z. Han, C. Zhang, G. Sullivan, A. Ikhlassi, K. Chang, and R.-R. Du, Phys. Rev. Lett. **119**, 056803 (2017).

[20] T. L. Schmidt, S. Rachel, F. von Oppen, and L. I. Glazman, Phys. Rev. Lett. **108**, 156402 (2012).

[21] J. C. Budich, F. Dolcini, P. Recher, and B. Trauzettel, Phys. Rev. Lett. **108**, 086602 (2012).

[22] N. Lezmy, Y. Oreg, and M. Berkooz, Phys. Rev. B **85**, 235304 (2012).

[23] J. I. Väyrynen, M. Goldstein, and L. I. Glazman, Phys. Rev. Lett. **110**, 216402 (2013); J. I. Väyrynen, M. Goldstein, Y. Gefen, and L. I. Glazman, Phys. Rev. B **90**, 115309 (2014).

[24] N. Kainaris, I. V. Gornyi, S. T. Carr, and A. D. Mirlin, Phys. Rev. B **90**, 075118 (2014).

[25] F. Crépin, J. C. Budich, F. Dolcini, P. Recher, and B. Trauzettel, Phys. Rev. B **86**, 121106 (2012); F. Geissler, F. Crépin, and B. Trauzettel, *ibid.* **89**, 235136 (2014).

[26] L. Kimme, B. Rosenow, and A. Brataas, Phys. Rev. B **93**, 081301 (2016).
[27] M. Kharitonov, F. Geissler, and B. Trauzettel, Phys. Rev. B **96**, 155134 (2017).
[28] Y. Tanaka, A. Furusaki, and K. A. Matveev, Phys. Rev. Lett. **106**, 236402 (2011).
[29] Q. Liu, C.-X. Liu, C. Xu, X.-L. Qi, and S.-C. Zhang, Phys. Rev. Lett. **102**, 156603 (2009); R. Žitko, Phys. Rev. B **81**, 241414(R) (2010); H.-M. Guo and M. Franz, *ibid.* **81**, 041102(R) (2010).
[30] E. Eriksson, A. Ström, G. Sharma, and H. Johannesson, Phys. Rev. B **86**, 161103(R) (2012).
[31] J. Maciejko, C. Liu, Y. Oreg, X.-L. Qi, C. Wu, and S.-C. Zhang, Phys. Rev. Lett. **102**, 256803 (2009).
[32] J. S. Van Dyke and D. K. Morr, Phys. Rev. B **93**, 081401(R) (2016).
[33] J. S. Van Dyke and D. K. Morr, Phys. Rev. B **95**, 045151 (2017).
[34] U. Fano, Phys. Rev. **124**, 1866 (1961).
[35] J. R. Schieffer, J. Appl. Phys. **38**, 1143 (1967).
[36] C. L. Kane and M. P. A. Fisher, Phys. Rev. Lett. **68**, 1220 (1992); Phys. Rev. B **46**, 15233 (1992).
[37] D. Yue, L. I. Glazman, and K. A. Matveev, Phys. Rev. B **49**, 1966 (1994).
[38] M. P. A. Fisher and L. Glazman in *Mesoscopic Electron Transport*, edited by L. Kowenhoven, G. Schön, and L. Sohn, NATO ASI Series E (Kluwer Academic Publishers, Dordrecht, The Netherlands, 1997).
[39] L. I. Glazman, I. M. Ruzin, and B. I. Shklovskii, Phys. Rev. B **45**, 8454 (1992).
[40] S.-J. Qin, M. Fabrizio, and L. Yu, Phys. Rev. B **54**, R9643(R) (1996).
[41] C. Rylands and N. Andrei, Phys. Rev. B **94**, 115142 (2016).
[42] Z. Yao, H. W. Ch. Postma, L. Balents, and C. Dekker, Nature (London) **402**, 273 (1999).
[43] A. O. Gogolin, A. A. Nersesyan, and A. M. Tsvelik, *Bosonization and Strongly Correlated Systems* (Cambridge University Press, Cambridge, UK, 1999); T. Giamarchi, *Quantum Physics in One-Dimension* (Clarendon Press, Oxford, UK, 2004).
[44] R. R. Nair, I.-L. Tsai, M. Sepioni, O. Lehtinen, J. Keinonen, A. V. Krasheninnikov, A. H. Castro Neto, M. I. Katsnelson, A. K. Geim, and I. V. Grigorieva, Nat. Commun. **4**, 2010 (2013); M. A. Khan, M. Erementchouk, J. Hendrickson, and M. N. Leuenberger, Phys. Rev. B **95**, 245435 (2017).
[45] B. Zhou, H.-Z. Lu, R.-L. Chu, S.-Q. Shen, and Q. Niu, Phys. Rev. Lett. **101**, 246807 (2008).
[46] G. Zhang, X. Li, G. Wu, J. Wang, D. Culcer, E. Kaxiras, and Z. Zhang, Nanoscale **6**, 3259 (2014).
[47] H. Doh, G. S. Jeon, and H. J. Choi, arXiv:1408.4507.
[48] M. Goldstein and R. Berkovits, Phys. Rev. Lett. **104**, 106403 (2010).
[49] I. V. Lerner, V. I. Yudson, and I. V. Yurkevich, Phys. Rev. Lett. **100**, 256805 (2008).
[50] Y. Meir and N. S. Wingreen, Phys. Rev. B **50**, 4947(R) (1994).
[51] V. Gurarie, Phys. Rev. B **83**, 085426 (2011).
[52] M. A. Cazalilla and J.-H. Zheng (unpublished).
[53] J. Cardy, *Scaling and Renormalization in Statistical Physics* (Cambridge University Press, Cambridge, UK, 1996).